Available online at www.sciencedirect.com
SCIENCE DIRECT®
International Journal of Heat and Fluid Flow 26 (2005) 695–708
International Journal of HEAT AND FLUID FLOW
www.elsevier.com/locate/ijhff

Unsteady loss in a high pressure turbine stage: Interaction effects

S.J. Payne [a,*], R.W. Ainsworth [a], R.J. Miller [b,1], R.W. Moss [c,1], N.W. Harvey [d]

[a] Department of Engineering Science, University of Oxford, Oxford OX1 3PJ, UK
[b] Whittle Laboratory, University of Cambridge, UK
[c] School of Marine Science and Technology, University of Newcastle upon Tyne, UK
[d] Rolls-Royce plc., Derby, UK

Received 17 December 2004; received in revised form 28 April 2005; accepted 29 April 2005
Available online 11 July 2005

Abstract

An investigation into the unsteady losses in a high pressure turbine stage has been performed experimentally at engine-representative conditions. This has been done by making time-resolved measurements of entropy at stage exit over all vane and rotor-relative positions over a wide range of radial height. These measurements provide a unique set of experimental data in that this is the first time that a full-field unsteady entropy survey has been attempted in a turbine facility capable of realistic Reynolds and Mach numbers. In a previous paper [Int. J. Heat Fluid Flow 24 (2003) 698] the exit flow of the rotor at one vane relative phase was reported. This allowed the loss associated with rotor flow features such as wakes, tip flows and secondary flows to be determined. The aim of this paper is to investigate the effects of vane–rotor interaction on both the time-mean and time-resolved performance of the stage. In addition to the experimental results, an unsteady Reynolds-averaged Navier–Stokes prediction of the flow field within the stage has been undertaken. Comparison of the experimental measurements with the prediction showed that time-mean efficiencies differ by 1.2%. The experimental results showed an unsteady change in stage efficiency of 1.2% as the rotor moves relative to the upstream vane. This was much higher than the 0.2% change predicted by the unsteady solver.

Keywords: Unsteady flow; Loss mechanisms; Entropy measurements; Efficiency; Interaction effects

1. Introduction

The flow field in the high pressure turbine stage is very complex, due to the high degree of unsteadiness and the effects of blade row interaction. There is still much experimental work to be performed before the unsteady loss mechanisms that occur in transonic high pressure turbines are understood. Although numerical predictions have been proved to be valuable in understanding the flow structure, it is important to gauge their accuracy in an absolute sense by comparison with experimental measurements, both for individual loss features and the stage efficiency. It is thus vital that experimental measurements are made at engine-representative conditions, to understand and to quantify the losses and to validate numerical predictions. This is the aim of this work presented here.

The efficiency of a turbomachine is usually defined as the ratio of the actual work output to the 'ideal' isentropic work output. The difference between these two is known as the lost work and in an adiabatic flow is proportional, for small changes, to the entropy generated by irreversibilities:

$$W_{\text{lost}} = T_{03}\Delta S_{\text{ir}}. \quad (1)$$

* Corresponding author. Tel.: +44 186 528 3306; fax: +44 186 527 3905.
E-mail address: stephen.payne@eng.ox.ac.uk (S.J. Payne).
[1] Formerly in the Department of Engineering Science, University of Oxford.

0142-727X/$ - see front matter © 2005 Elsevier Inc. All rights reserved.
doi:10.1016/j.ijheatfluidflow.2005.04.005

Nomenclature

n	constant
p	pressure
s	specific entropy
u	velocity
A	area; constant
B	constant
C	constant
D	constant
E	voltage
M	Mach number
N	rotational speed
Nu	Nusselt number
R	gas constant
Re	Reynolds number
T	temperature
W	work
γ	ratio of specific heats
η	efficiency; recovery factor
ρ	density

Subscripts

ir	irreversible
lost	lost
m	mean
r	ratio
w	wall; wire
0	total conditions
1	HP vane inlet conditions
2	HP vane exit conditions
3	HP rotor exit conditions

Superscripts

–	mean
*	choked

For an adiabatic flow, the entropy can be said to be a measure of the 'quality' of the energy and thus an increase in entropy leads directly to a reduction in the work potential of the fluid.

An additional advantage of entropy for studying losses in turbomachines is that it is independent of the frame of reference of the measurement. The efficiency of a turbine stage can thus be determined from the total entropy creation and one other property of state:

$$\eta = \frac{1 - \left(p_{\mathrm{r}} \mathrm{e}^{(s_2 - s_1)/R}\right)^{\frac{\gamma-1}{\gamma}}}{1 - \left(p_{\mathrm{r}}\right)^{\frac{\gamma-1}{\gamma}}}. \tag{2}$$

The disadvantages of using entropy are that it cannot be measured directly and that only changes in entropy have any meaning, necessitating the measurement of four flow parameters:

$$\frac{s_2 - s_1}{R} = \left(\frac{\gamma}{\gamma - 1}\right) \ln\left(\frac{T_{02}}{T_{01}}\right) - \ln\left(\frac{p_{02}}{p_{01}}\right). \tag{3}$$

We assume throughout this paper that the working fluid, air, is an ideal gas.

There are three fluid dynamic processes that create entropy, and hence loss: viscous friction, heat transfer and non-equilibrium processes, such as the very rapid expansions that occur in shock waves, Denton (1993). A review of the different loss components was given in Payne et al. (2003) and is omitted here for brevity. However, despite our often relatively good understanding of the flow field, the accuracy of loss predictions is still low, as the entropy generation cannot be estimated accurately. Although numerical predictions are valuable in predicting the flow structure, there are difficulties in predicting the loss accurately, due to errors in predicting the boundary layers, transition and the base pressure coefficient, as well as those due to entropy generation due to numerical dissipation. There are also very few experimental measurements of unsteady loss at engine-representative conditions with which to validate either loss correlations or numerical predictions.

Under engine-representative conditions, blade row interaction effects are likely to have a significant effect as the flow field exiting one blade row cannot mix out completely before entering the next blade row; the unsteadiness thus affects both rows. The rotation of alternate blade rows also introduces unsteadiness.

Unsteady blade interaction is likely to affect performance in three ways. Firstly, the three-dimensional non-uniform flow from an upstream vane mixes out as it passes though the downstream rotor blades. Depending on the vortical content of the flow, the preferential and adverse pressure fields in the rotor cause either a rise or a fall in the associated mixing losses. Secondly, the interaction of the blade rows can alter either the state of the rotor boundary layer or the freestream velocity at the edge of the boundary layer. Both of these can lead to large changes in the creation of the entropy in the boundary layer. Thirdly, blade interaction can alter the way in which the rotor flow phenomena, such as the end wall flows and tip flows, develop and thus change rotor end wall and tip losses.

Blade row interaction can be subdivided into a number of different effects, each of which is outlined briefly. Wake interaction is the dominant interaction in terms of loss generation and occurs as the wake is chopped up into segments as it passes through the downstream blade row. This effect has been examined by Hodson and Dawes (1998), Zaccaria and Lakshminarayana (1997)

and Binder et al. (1989) amongst others. In a turbine rotor, the core flow is accelerated. Mixing in a preferential pressure gradient lowers the mixing loss of the upstream wake. Shock wave and potential field interactions have been studied by Collie et al. (1992), Johnson et al. (1989) and Korakianitis (1993) amongst others. If a laminar flow exists on the early rotor suction surface, the presence of the shock interaction is likely to cause early transition of the flow and thus increase loss. The boundary layer loss varies with the cube of the freestream velocity and so an oscillating rotor velocity field is likely to cause higher total boundary layer loss than the corresponding time-averaged flow, due to the non-linearity.

Secondary flow interaction is caused by the secondary flow structure from the upstream vane being cut by and convecting through the rotor. The hub and casing secondary flows contain streamwise, radial and tangential vorticity. The mixing losses associated with each of these will depend upon the nature of the interaction between the blade rows.

In the secondary flow interaction, vortices are convected through the downstream blade rows similarly to wakes, but the effects on the loss are much greater, Denton (1993). There are two mechanisms for the breakdown of a secondary flow vortex: cutting of the vortex by fluid which flows into the previously low pressure core, and bowing of the vortex as it passes through the rotor passage. Following the cutting of the wakes and the stator secondary vortices, the random unsteadiness is increased considerably in the regions associated with the secondary flow, Binder (1985). Numerical predictions have shown that the efficiency increases when the unsteady flow processes occur upstream of the rotor leading edge rather than in the downstream blade row, Jennions and Adamczyk (1997).

Although a considerable amount of research has been performed on studying individual interaction mechanisms, little work has been performed at engine-representative conditions, due to the difficulty in obtaining relevant experimental measurements. The general level of understanding of interaction is thus still far behind that of the losses in isolated blade rows.

Miller et al. (2003b) used unsteady total pressure, Mach number and flow angle measurements to study blade row interaction in a transonic turbine. As a result of this study, two interaction phenomena were postulated: the two-dimensional interaction phenomenon and the hub interaction phenomenon. The first affects the rotor exit flow simultaneously over the whole radial height, modulating the wake depth and width but not significantly altering the rotor trailing edge shock strength, whilst the second causes the hub region to alternate between subsonic and supersonic flow, thus periodically removing the trailing edge shock. It was suggested that the first was caused by shock interaction, since this is largely independent of radial height, whereas the second was caused by vane wake interaction, since the wake leans over and migrates towards the hub end wall, periodically merging with the rotor hub secondary flow. However, without measuring unsteady entropy, these could not be confirmed and their effects on the loss could not be calculated. A previous paper, Payne et al. (2003), presented experimental measurements of entropy in the same facility at a single vane phase, i.e. with a stationary probe. The experimental results presented here, unsteady entropy over all vane positions, are intended to provide the necessary measurements for the understanding of interaction effects on the loss mechanisms in this turbine.

2. Experimental facility

In order to make relevant and accurate unsteady loss measurements, the necessary flow conditions must be modelled correctly. The facility used here is the Oxford Rotor Facility, which was designed to simulate engine-representative conditions by matching the required non-dimensional conditions for a very short period of time, Ainsworth et al. (1988). The working section comprises a 0.62 scale version of the Rolls-Royce RT27a blade profile for the high pressure (HP) turbine stage and the first blade row from a typical intermediate pressure (IP) stage, Fig. 1. Since the rotor is unbraked and thus continuously accelerating, the facility is at the required flow conditions for only approximately 15 ms. Each traverse was completed in the 15 ms using an ultra-high speed traverse mechanism driven by a large compression spring, Miller and Ainsworth (1996).

Dimensional analysis shows that there are only four dependent parameters that must be matched to simulate the required engine-representative conditions, Sheard

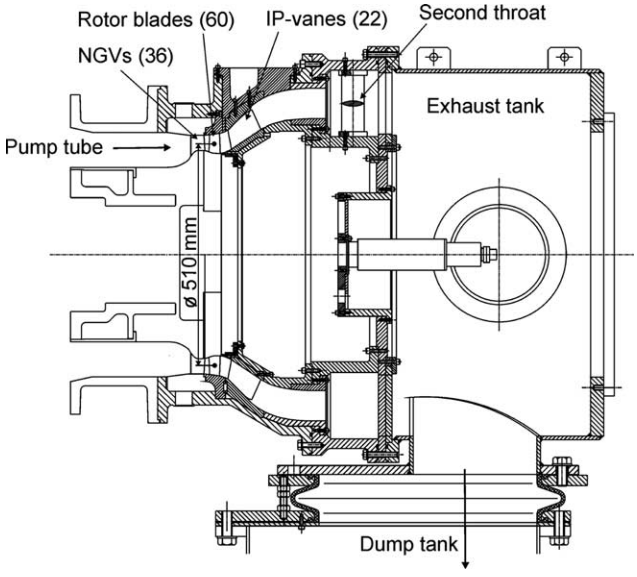

Fig. 1. Oxford rotor facility working section.

Table 1
Pseudo non-dimensional operating point parameters

Specific speed	Pressure ratio	Reynolds number	Temperature ratio
$\frac{N}{\sqrt{T_{01}}}$	$\frac{p_{01}}{p_3}$	Re_2	$\frac{T_{01}}{T_w}$
460.49 rpm/$\sqrt{K}$	3.12	2.7×10^6	1.3

(1989). Removal of the parameters that remain unchanged from each run gives the necessary pseudo non-dimensional operating point parameters, Table 1. The Nozzle Guide Vane exit Reynolds number is based on absolute conditions and the axial chord. The gas-to-wall temperature ratio is chosen to be 1.3, based on a compromise between run time and the magnitude of piston oscillations, Ainsworth et al. (1988).

It was shown in Payne et al. (2003) that the entropy due to heat transfer can be safely neglected in comparison with the entropy due to loss. This is important, since the aim here is to use the entropy measurements to interpret the loss structure, rather than necessarily to estimate the actual rise in entropy. It is not known what the effects of a different gas-to-wall temperature ratio would be on the entropy gain. In addition, the turbulence of the flow entering the HP turbine is of order 2.5%, Ainsworth et al. (1988), and the flow field is approximately uniform across the passage. Although neither of these would be expected in a real engine, the focus here is on the losses in the HP turbine stage, so the flow field entering the turbine is kept as uniform as possible to facilitate interpretation of the experimental results relative to the performance of the HP turbine.

In parallel with the experimental measurements, considerable work has been performed on numerical predictions of the flow field. When taken together, they provide a development cycle: the predicted flow structure can be used to aid the interpretation of the experimental results, which in turn evaluate the accuracy of the predictions. This is of crucial importance for the loss, since the code must be able to predict loss accurately if apparent improvements in efficiency are to be used as a basis for choosing an improved design.

The code used here, Unstrest, is three-dimensional, viscous and unsteady. It solves a thin shear layer model of the Navier–Stokes equations with the viscous terms evaluated every time step and turned into body force terms for momentum and source terms for energy. The structured grid is formed by the rotation of points defined in two dimensions about the turbine axis: meridional, i.e. pseudo-streamwise, and pseudo-radial. The code uses a 'time-marching' solution scheme in which one blade row gradually rotates relative to the other with flow parameters being interpolated across a sliding plane between the two grids, Denton (1992). The version of Unstrest used here was developed by Denton but includes some modifications made at Rolls-Royce plc.

The prediction used here, the same as in Payne et al. (2003), has been run at the correct operating conditions with the correct vane–rotor blade ratio of 3:5 and contains approximately 1.6 million nodes. The 2.25% tip gap/span is also modelled: this is important for assessing the impact of the tip leakage flow on the stage efficiency. Since the focus here is on the interaction of the loss mechanisms between the HP nozzle guide vanes and the HP rotor, the downstream vane and swan-necked duct have been omitted.

3. Instrumentation

Since entropy cannot be measured directly, two properties of state are required: normally total pressure and total temperature, Eq. (3). Although the measurement of total pressure at a high bandwidth is a well-established technique, it has proved to be considerably harder to measure total temperature at a similar bandwidth. The aspirating probe was thus originally designed to measure unsteady total temperature at high frequencies, Ng and Epstein (1983). Although thin film heat transfer gauges, Buttsworth et al. (1998), are now an alternative method of measuring total temperature at high frequencies, the aspirating probe remains the only means of simultaneously measuring total pressure and total temperature both spatially and temporally. This is crucial in obtaining the necessary measurement accuracy, as was shown in Payne et al. (2003). The other advantages associated with the aspirating probe include a high frequency response, good spatial resolution, small sensitivity to flow angle and a reduction in the effects of probe blockage.

The aspirating probe essentially consists of two hot wires placed side by side upstream of an orifice, Fig. 2. By maintaining a low pressure downstream of the

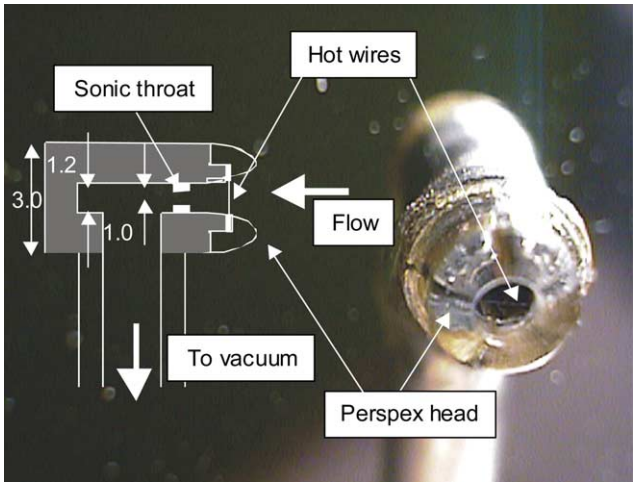

Fig. 2. Oxford aspirating probe design, dimensions in mm.

orifice, it is choked and the probe 'sucks' in the flow approaching it. By calculating the mass flow for a given total pressure, total temperature and Mach number, the mass flow at the choked orifice and the hot wire plane can be equated to give

$$(\rho u)_{\mathrm{w}} = \sqrt{\frac{\gamma}{R}}\frac{p_0}{\sqrt{T_0}}\frac{A^*}{A_{\mathrm{w}}}\left(\frac{2}{\gamma+1}\right)^{\frac{(\gamma+1)}{2(\gamma-1)}}. \quad (4)$$

The Reynolds number at the hot wire plane is thus dependent solely upon the total pressure and total temperature. The Mach number is fixed by the area ratio:

$$M_{\mathrm{w}}\left(1+\frac{\gamma-1}{2}M_{\mathrm{w}}^2\right)^{-\frac{(\gamma+1)}{2(\gamma-1)}} = \frac{A^*}{A_{\mathrm{w}}}\left(\frac{\gamma+1}{2}\right)^{-\frac{(\gamma+1)}{2(\gamma-1)}}. \quad (5)$$

For a hot wire used with constant temperature anemometry in a constant Mach number flow, the Nusselt number is solely dependent upon the Reynolds number, see for example Bruun (1995). When placed inside the aspirating probe, hot wires can thus be used to measure the Reynolds number, using the general relationship between Nusselt number and Reynolds number for a given Mach number, Collis and Williams (1959):

$$Nu = A + BRe^n. \quad (6)$$

When combined with the standard hot wire equation, this gives the aspirating probe calibration equation:

$$E^2 = \left[C\left(\frac{p_0}{\sqrt{T_0}}\right)^n + D\right](T_{\mathrm{m}} - \eta T_0), \quad (7)$$

where the recovery factor, η, is the ratio of recovery temperature to total temperature and C, D and n are constants. These constants are all found by calibration, despite η being a known function of Mach number, to give the greatest accuracy. Two hot wires are thus required to measure both total pressure and total temperature. Although the wire temperatures should be far apart to give a high level of measurement accuracy, there is a lower limit due to the need for a high bandwidth and an upper limit due to the melting temperature of the wire.

The basic design of the aspirating probe used here follows that of Ng and Epstein (1983) with the probe being made as small as possible to fit between closely coupled blade rows. Platinum-plated tungsten wire of diameter 5 μm was used, since this is less prone to drift and has a high yield strength and temperature coefficient of resistance: all of which improve the measurement accuracy. The wire length to diameter ratio was 240, to reduce conduction effects whilst keeping a high spatial resolution. The wires were placed perpendicular to the rotor trailing edge and were less than 0.5 mm apart. The Mach number at the hot wire plane was set at the mean rotor exit value of 0.45 to reduce blockage effects. The probe head was made of Perspex, giving the smoothest possible both internal and external probe surfaces, thus preventing any spurious local entropy generation and improving the angle sensitivity. Although we have not tested the aspirating probe for the effects of variations in flow angle, the findings of Ng and Epstein (1983) that there is negligible change in probe behaviour as the flow angle is varied within ±20° at the correct freestream Mach number indicate that this effect is small outside the tip region.

The wire temperatures were set at approximately 350 and 550 K to give the greatest measurement accuracy, the mean total temperature at the measurement plane being approximately 295 K. To remove noise and to ensure that the bandwidths of the two hot wires were equal, all the data was filtered using a 100 point FIR low-pass filter with a cut-off frequency of 40 kHz: approximately the bandwidth of the lower temperature hot wire.

The probe is calibrated using a dedicated chamber designed and built by Brayton (1996), which allows wide ranges of total pressure and total temperature to be set independently. By taking a set of data points in the range 2–4 bar and 20–40 °C, a least-squares-error approach is used to provide a fit to the calibration equation. A detailed analysis of all the possible sources of error has shown that the rms errors in total pressure and total temperature are approximately 0.80% and 0.14% respectively: since the Mach number is constant, these are also the rms errors in pressure and temperature. These errors correspond to standard deviations in entropy/R and stage efficiency of 0.013% and 1.2%, for a stage total pressure ratio of 2.5, Payne (2001). Since errors in total pressure and total temperature magnify noticeably when transformed into efficiency, great care has to be taken to ensure that entropy measurements are sufficiently accurate to resolve loss features.

There is a significant high frequency effect in hot wire anemometry, due to the attenuation of heat transfer by conduction from the hot wire to the probe supports, Parantheon et al. (1983). A theoretical examination of this effect has led to the derivation of a compensation factor, which must be used when measuring flow phenomena above a frequency of approximately 1 Hz. When the hot wires are placed inside the aspirating probe, there is a second high frequency effect, due to the fluctuations in the flow field inside the probe being constrained by a constant throat Mach number. This effect cannot be predicted easily and has thus been measured experimentally, leading to an aspirating probe transfer function that must be inverted when processing the measurements made with the aspirating probe. This is outlined in more detail in Payne (2001).

Relatively few authors have ever used an aspirating probe to measure entropy and these did so primarily in compressors running at lower speeds than are typical in the Oxford rotor facility. These include Ng and Epstein (1985) and Alday et al. (1993), where the wake

region was shown by a rise in entropy, although an extra semiconductor probe was required to give more accurate results. This extra probe was shown by Van Zante et al. (1995) to be unnecessary if care was taken in the design and calibration of the aspirating probe. Van Zante et al. (1995) also presented stationary measurement of total pressure and total temperature, but did not present entropy: likewise Suryavamshi et al. (1996), although they calculated the local isentropic efficiency. Similarly Brouckaert (1998) used the aspirating probe in the facility at VKI behind a turbine stage at higher rotational speeds without attempting to present entropy traces. Thin film heat transfer gauges were used in conjunction with a semiconductor pressure probe by Buttsworth et al. (1998) but again only to present total pressure and total temperature. There were thus no accurate entropy traces at the high frequencies found in turbomachines prior to those measurements presented by Payne et al. (2003). Those experimental measurements are now complemented here by the inclusion of the effects of blade row interaction, providing a unique and comprehensive set of data.

Before presenting the experimental data, it should be noted that experimentation is vital in improving our understanding of the complex and poorly understood effects of interaction, yet, inevitably they are confined to a particular blade geometry for a given experiment. The nature of the experimental facility used here is such that the results presented here are representative of the interaction effects found in turbines, and the discussion that follows focuses on the general nature of these effects, rather than on what necessarily occurs for a particular blade geometry. Future work will be required to examine precisely how dependent the results presented here are on the blade geometry.

4. Three-dimensional rotor dependent flow structure

The experimental results presented in Payne et al. (2003) clearly show that there are four major loss features at rotor exit: tip leakage vortex, upper passage vortex, wake and lower passage vortex, Fig. 3. The formation of the loss structure through the rotor blades was also shown by the numerical prediction, Fig. 4. The inlet boundary layer is rolled up into passage vortices on the end walls. The upper passage vortex is reduced in size by the presence of the rotor tip gap. As the vortex passes through the rotor, it starts to orbit around the rotor tip leakage flow, dissipating in strength. The radial pressure gradient causes high loss, low momentum fluid to migrate radially outwards and hence the lower part of the wake is rolled up into the lower passage vortex, resulting in little wake fluid being found close to the hub end wall. It should be noted that the trailing edge shock cannot be seen in Figs. 3 and 4. This is due to the shock wave generating very little entropy as it is very weak.

It was shown in Payne et al. (2003) that the numerically predicted stage efficiency was in very good agreement with both the experimentally derived value and the value measured in a cold rig test. Both experiment and prediction found that the primary flow entropy was the largest source of loss. When the losses associated with the wake, tip leakage flow and lower passage vortex were analysed separately, some differences were

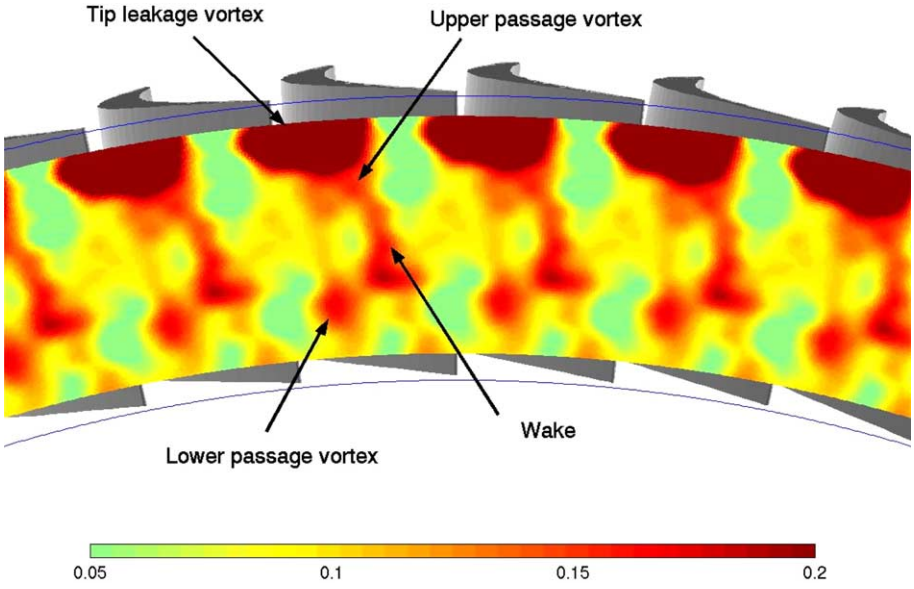

Fig. 3. Experimental entropy/R contour plot at 30% vane position, from Payne et al. (2003).

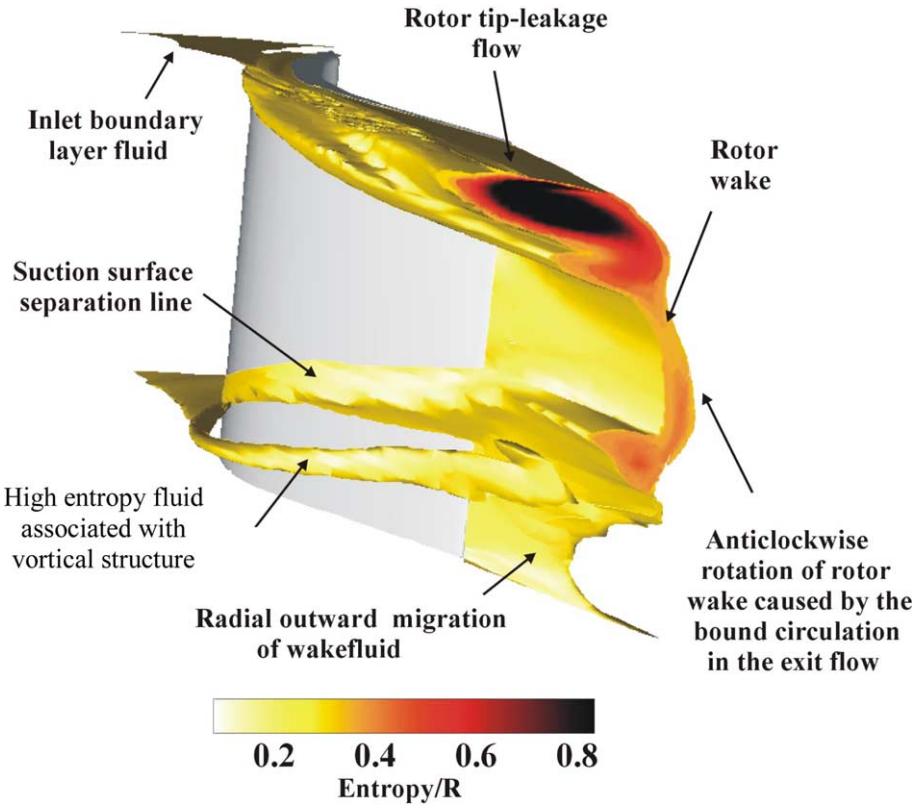

Fig. 4. Numerical prediction of formation of loss structure, from Payne et al. (2003).

observed. Both experiment and prediction showed that the primary flow entropy was the largest source of loss. The entropy generation in the tip leakage flow was in good agreement, whereas the predicted levels in the wake were larger than the experimentally derived values. These comparisons will be examined in more detail in this paper than was previously possible, using the measurements over the entire vane phase.

5. Three-dimensional rotor and vane dependent flow structure

The measurements of entropy at a single vane position over all radial heights clearly show the basic loss structure. To investigate the effects of vane interaction, the aspirating probe was then traversed across the entire vane phase at the same radial heights, thus providing the complete time-resolved loss structure over all radial and circumferential positions. Since these unsteady measurements are difficult to interpret on the printed page, they will be presented by means of the phase–phase interaction diagram, Miller et al. (2003a).

This uses the co-ordinate system defined in Fig. 5, where both the rotor and vane phases are defined as varying from 0 on the suction to 1 on the pressure surface side of the trailing edge. At each radial height, the flow

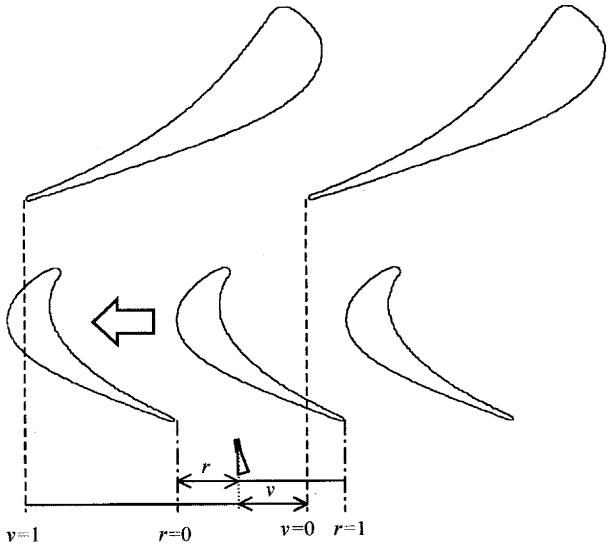

Fig. 5. Vane and rotor co-ordinate systems.

parameters can be interpolated onto a grid of rotor and vane phases. These are then plotted as a series of planes, one for each radial height, where the horizontal axis is taken to be the vane phase and the vertical axis the rotor phase. The unsteady measurements of entropy over all rotor and vane phases at a series of approximately uniformly spaced heights are thus shown in

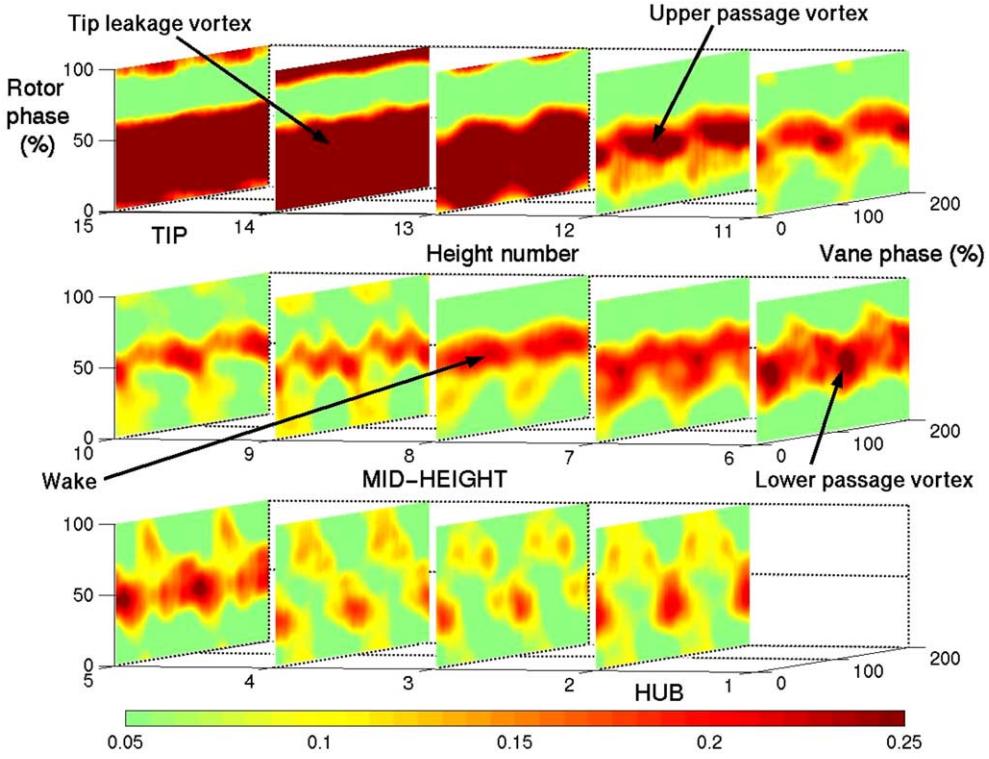

Fig. 6. Aspirating probe phase–phase diagram for vane-dependent entropy/R.

Fig. 6, where height 15 is closest to the tip, height 1 to the hub.

For any given plane (i.e. at a particular radial height), the surface represents how the flow field across the circumference varies with relative vane position and relative rotor position. A stationary probe would measure the flow field represented by a vertical line on the phase–phase plane, where the vertical axis represents rotor relative position and can thus be directly be related to time, whereas a rotor-mounted probe would measure that represented by a horizontal line. The key advantage of plotting the data in this format is that the effects of vane interaction can easily be seen. If there are no vane interaction effects, the flow features will be seen as purely horizontal stripes (i.e. every vertical line on a particular phase–phase plane would be identical and a stationary probe would measure the same flow variation whatever its circumferential position). Alternatively, if the flow field is independent of the rotor, the flow features will be seen as vertical stripes.

The four loss mechanisms shown in Payne et al. (2003) are clearly seen in Fig. 6. Over most of the radial heights, the flow field is predominantly rotor-dependent, as shown by the horizontal stripes. This only changes close to the hub, providing evidence of the presence of the hub interaction phenomenon proposed by Miller et al. (2003a). The effects of blade row interaction on each of the loss features will now be presented and compared with the numerical predictions before the effects of interaction on the stage efficiency are assessed.

6. Tip leakage vortex

The main effect of vane interaction on the tip leakage vortex is a modulation of its size and depth as the rotor blades move relative to the upstream vanes. However, the size of this modulation is found to be small, as seen in Fig. 6 for heights 13–15. This is also shown in Fig. 7, where the variation of entropy/R is shown over rotor phase at height 15 (93%). To illustrate the variation with vane phase, at each rotor phase the mean and standard deviation values over vane phase of entropy/R are calculated: Fig. 7 shows the mean, the mean plus one standard deviation and the mean minus one standard deviation values. The tip leakage flow is driven by the pressure difference across the tip gap: this pressure difference being varied by the vane trailing edge shock. However, these results indicate that the vane trailing edge shock has little effect on the formation of the rotor tip leakage flow since there is little variation over vane phase. Miller et al. (2003b) showed that vane interaction only affected the rotor pressure field upstream of the rotor crown, whereas the formation of the tip leakage flow is strongest downstream of the crown, and this is supported by the data presented here.

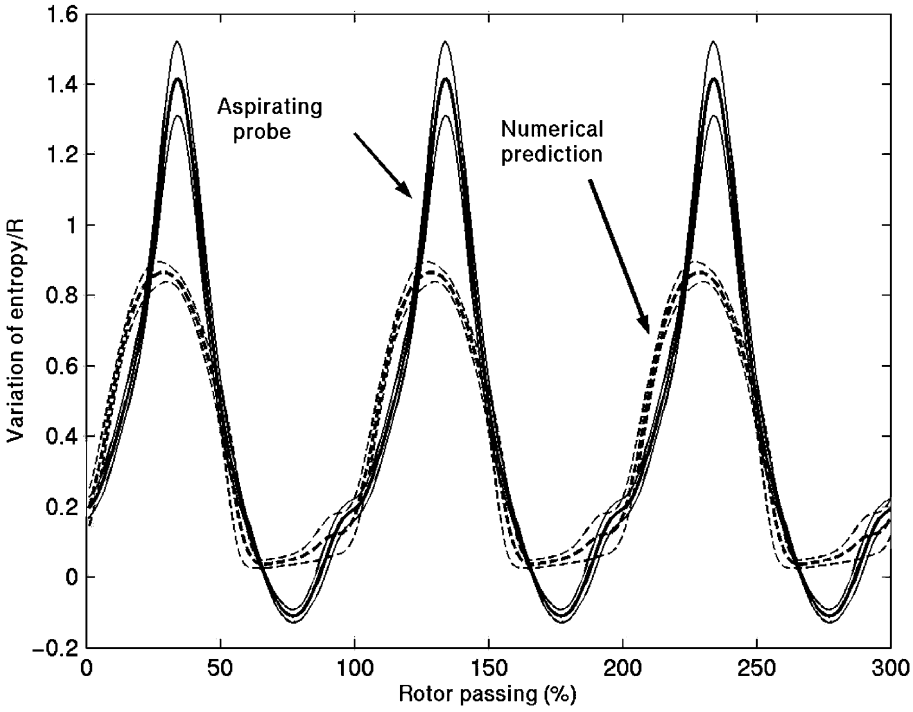

Fig. 7. Ranges of entropy/R over vane position against rotor position at height 15 (93%).

The variation in predicted entropy/R shows good general agreement with the experimental measurements, as was previously shown in Payne et al. (2003). The net entropy generation is very similar, as is the small variance with vane phase, although the entropy is predicted to be slightly flatter over rotor phase than was measured. The mesh used in the numerical prediction, however, has only six elements across the tip gap and thus is unlikely accurately to predict the loss mechanisms due to the tip gap. The quality of the agreement found here is thus very encouraging.

7. Wake

The main effect of vane interaction on the wake is a modulation of the wake depth, width and position. The effect on the loss is difficult to quantify since the radial height range over which the wake is clearly observed is small. This is because close to the tip it interacts with the upper passage and tip leakage vortices and close to the hub it interacts with the lower passage vortex. Fig. 8 shows the rotor exit flow close to mid-height (height 9; 54% height) at two vane relative locations, corresponding to 30% and 80% vane relative phase. These locations correspond to the points with maximum entropy difference in the main flow, i.e. outside the wake. The increase in entropy due to the wake is clearly seen at all vane phases, Fig. 6: although the effects of blade row interaction on entropy are significant, the wake always has a higher value of entropy. It should be noted that the stationary measurements in Payne et al. (2003) were made at 30% vane phase, i.e. the point of minimum interaction. The computation over-predicts the wake depth and this is not discussed further in this paper as the over-prediction is common in transonic machines, Miller et al. (2003a).

Measurements of the total pressure deficit associated with the rotor wake for the same blade rows, Miller et al. (2003b), showed good agreement with measurements made in a linear cascade of the same rotor geometry by Mee et al. (1992). The latter results showed a total pressure deficit of approximately 8%, which corresponds to an entropy/R rise of 0.08. The measured entropy/R difference between the wake and mid-passage flow at 30% vane phase, i.e. minimum interaction, Fig. 8, is very similar to this value. The effects of blade row interaction on the wake can thus be quantified relative to the point of minimum interaction.

The variations in the wake maximum entropy/R, width and position with vane phase at 54% radial height are shown in Fig. 9. The position of the wake is defined here to be the rotor phase at which the maximum entropy/R occurs; the width to be the extent within which the entropy/R is greater than 0.01 below the maximum value. Although this latter definition is somewhat arbitrary it allows comparisons to be made about how spread out is the wake. The maximum entropy/R in the wake modulates between 0.13 and 0.22, its width between 6.7% and 12.1% and its position between 41% and

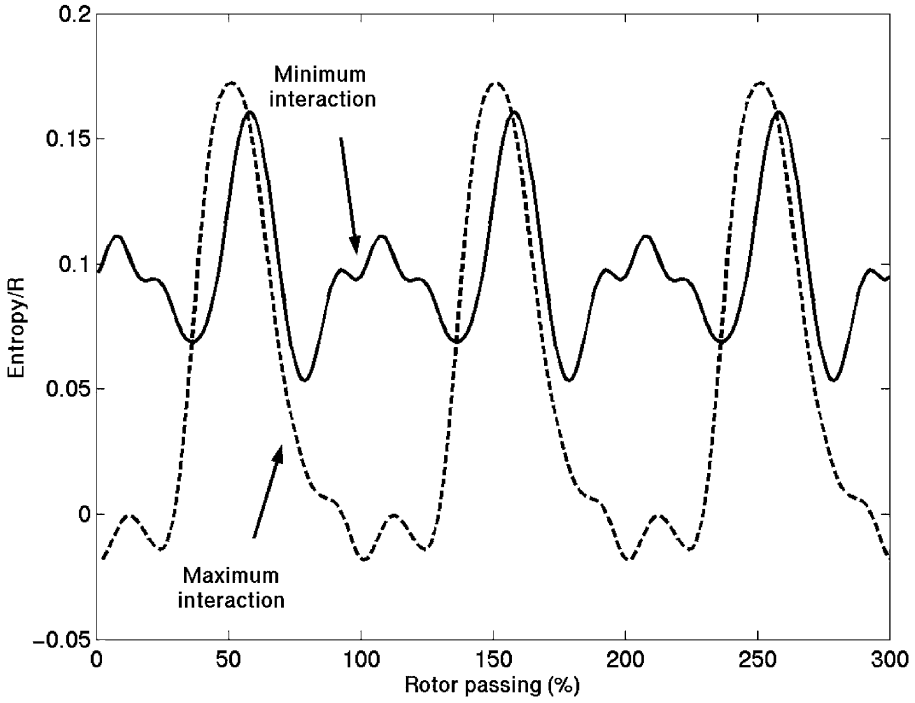

Fig. 8. Variation in entropy/R with rotor position at 30%, 63% and 96% vane position.

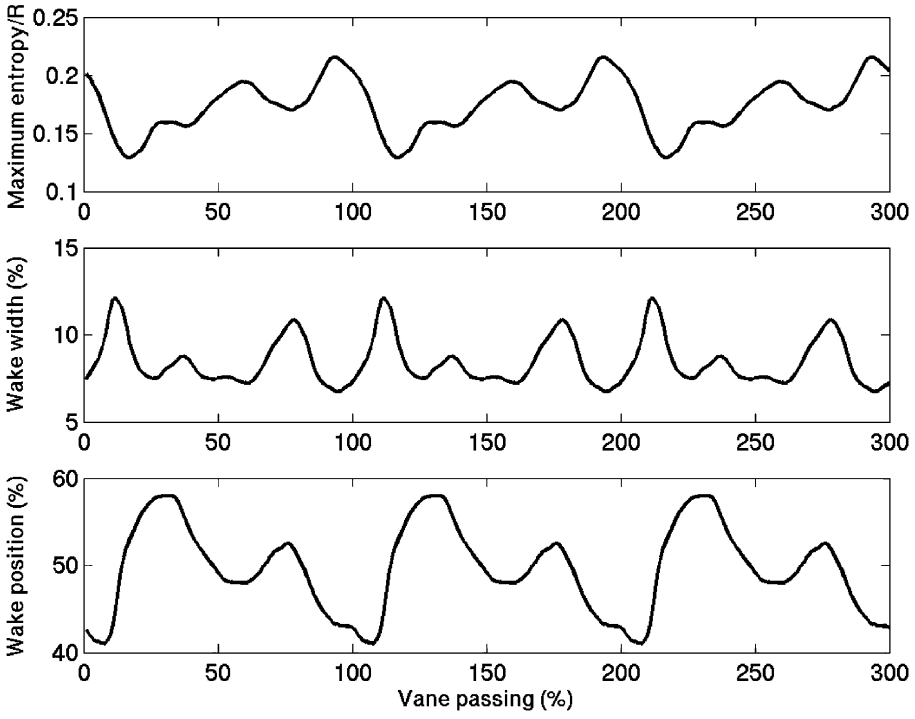

Fig. 9. Variation in wake depth and position with vane position.

58%. Interaction effects thus have a significant effect on the height and width of the wake, but less so on its position. There seems to be a correlation between an increase in the maximum entropy/R associated with the wake and a reduction in the rotor phase at which this occurs: for example, the minimum peak value occurs at approximately 20% vane phase corresponding to the maximum value of position. Miller et al. (2003a) showed

a similar variation in wake width and phase to Fig. 9: the wake width changing by 50% at 16% vane phase with smaller rises at approximately 40% and 75% vane phase. These are clearly shown in Fig. 9, where there are local increases in wake width at approximately 20%, 35% and 80%. These results imply that the changes in the total pressure depth of the mid-height rotor wake found by Miller et al. (2003a) were due to the vane exit entropy.

8. Lower passage vortex

There are two regions of high entropy fluid associated with the rotor hub secondary flow, as seen in Fig. 4. The first is caused by the pulsation of the high entropy, high loss fluid associated with the suction surface separation line. This is clearly shown at heights 6–5, Fig. 6, where the stripe of high entropy at approximately 50% rotor phase fluctuates considerably in strength with vane phase. This strengthening is greatest at approximately 0–30% vane phase, due to the hub interaction phenomenon, whereby the upstream vane wake or hub passage vortex periodically merges with the lower passage vortex. Due to radial migration, there is little high loss fluid below this: the vortices rise from hub to tip, as shown in Fig. 4. The second region of high entropy fluid is caused by the pulsation of the high loss fluid at the centre of the lower passage vortex, heights 4–2: this has a peak value at 0% vane phase at height 2. For vane phases in the approximate range 20–80% there is little high loss fluid seen. The effects of blade row interaction are thus clearly seen in the phase–phase diagram.

9. Time-mean flow field

The time-mean flow field is important since it determines the steady flow field at inlet to the downstream blade row. The time-mean entropy, Fig. 10, shows a large variation across vane phase over most of the radial height. The largest variation was found to be between 30% and 50% height, in agreement with the hub interaction phenomenon proposed by Miller et al. (2003a). The vane relative phase at which the high entropy fluid occurs, however, is different from the phase of the maximum total pressure deficit reported by Miller et al. (2003a). As the flow convects further downstream, low momentum, high loss fluid migrates towards the tip. The region of highest loss is thus likely to enter the downstream vane close to mid-height. This is important to consider when designing the downstream blade rows.

10. Stage efficiency

Following on from a qualitative assessment of the loss structure and the effects of blade row interaction, a quantitative assessment of the effects of the sources of loss on the stage efficiency can be made, which will also provide a quantitative estimate of the accuracy of the numerical loss predictions. This is vital in improving blade design and in validating the use of numerical predictions to predict blade efficiency. It should be noted that there is insufficient experimental data available to calculate the mixed-out losses and therefore only the entropy production upstream of the measurement plane has been considered here.

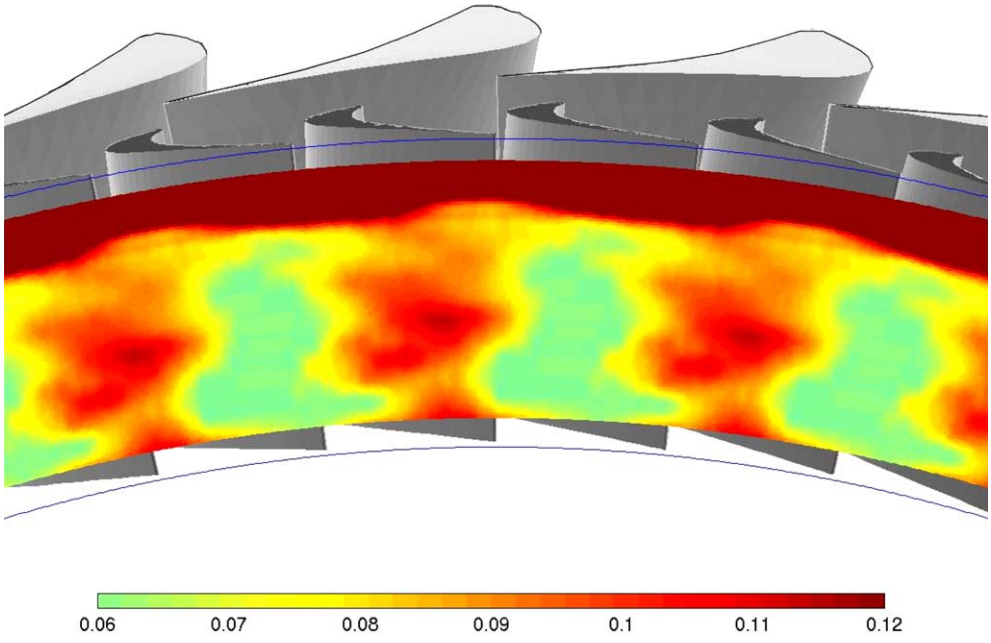

Fig. 10. Time-averaged entropy/R.

To quantify the different sources of loss, the flow field is divided into three regions: the primary flow, where the entropy is below a certain threshold value, the tip leakage flow and the remainder of the rotor loss flow field, comprising mainly the wake and lower passage vortex. Since the rotor loss mechanisms are associated with regions of low velocity fluid, the contributions of the entropy rise to the drop in efficiency must be mass-weighted:

$$\frac{\bar{s}}{R} = \frac{\int \left(\frac{s}{R}\right).\rho u.\mathrm{d}A}{\int \rho u.\mathrm{d}A}. \tag{8}$$

Since there is no experimental measurement of the mass flux, this data has to be provided by the numerical calculations. The spatial agreement in the flow structure was considered sufficient for this process. Close to the end walls, where no experimental data is available, the numerical predictions have also been used. Once the mean primary flow entropy has been calculated, the entropy in the remaining flow regions above this value is mass-averaged over the blade passage. This procedure is then performed for both the measurements and the predictions at each vane phase, to assess the effects of vane phase on the stage efficiency, for both the measurements and the predictions, Fig. 11 and Table 2. The flow field is thus averaged out over the rotor passage for each vane phase in turn. Note that the results obtained in this manner are approximate, but, in the absence of further experimental information, are the best estimate available: without entropy, however, no serious attempt could be made to estimate efficiency.

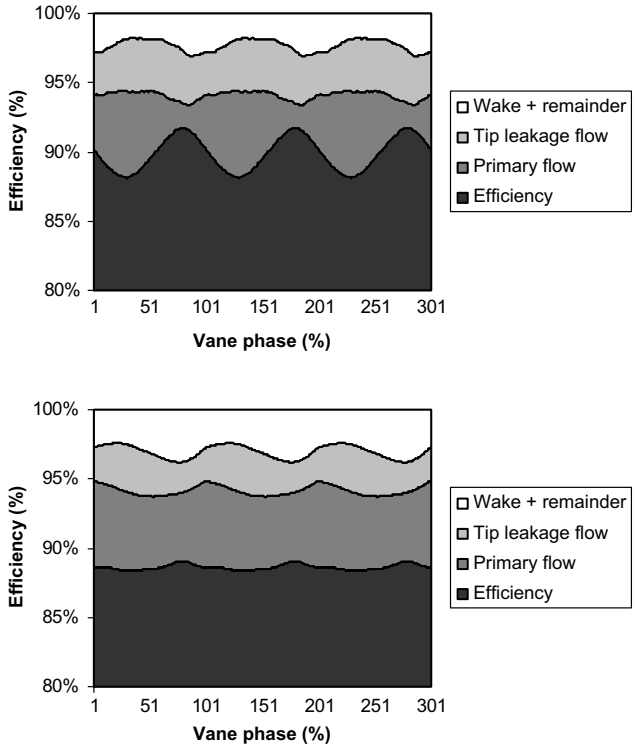

Fig. 11. Breakdown of efficiency variation with vane position: (a) experimental and (b) numerical prediction.

Table 2
Efficiency drops due to different regions of the flow field

	Aspirating probe	Numerical prediction
	Mean (std)	Mean (std)
Primary flow	4.20% (1.51%)	5.51% (0.39%)
Tip leakage flow	3.61% (0.31%)	2.80% (0.45%)
Remainder of loss	2.31% (0.46%)	3.05% (0.49%)
Total loss	10.13% (1.22%)	11.36% (0.20%)
Stage efficiency	89.87% (1.22%)	88.64% (0.20%)

The standard deviation in efficiency with vane phase, averaged over the whole height, is 1.2%. The numerical prediction significantly under-predicts this vane interaction, showing a standard deviation of only 0.2%. In terms of the time-mean values, the prediction is 1.2% lower than the experimental value. The vane phase used in Payne et al. (2003), 30%, proves to be where the efficiency is lowest, thus illustrating the need for measurements of efficiency over all vane phases. The measurements presented here thus supersede those presented in our earlier paper.

The experimental efficiency estimates suggest that the primary flow entropy generation varies the most, fluctuating with a standard deviation of 1.5% about a mean level of 4.2%. The tip leakage flow causes a largely constant efficiency drop of 3.6%, with a standard deviation of only 0.3%. The small standard deviation is expected, since the tip leakage vortex has consistently been shown to be almost invariant with vane phase, and is in excellent agreement with the findings in Payne et al. (2003). The vane averaged tip leakage efficiency drop is slightly closer to the expected value of 5.2% than the value at a single vane phase reported by Payne et al. (2003). The remainder of the secondary flow losses, however, are slightly more vane dependent, with a standard deviation of 0.5% about a mean of 2.3%.

Since the stationary measurements reported in Payne et al. (2003) reported the minimum efficiency drop, as well as the maximum primary flow efficiency drop, the relative importance of the remainder of the secondary losses on the stage efficiency was considerably underestimated. The importance of measuring the complete vane and rotor dependent flow field is again clearly demonstrated.

The drops in efficiency due to the tip leakage flow, wake and secondary flow are in good agreement with the numerical predictions, Fig. 11. The primary flow, however, shows a clear difference. The mean levels of efficiency drops are also in reasonable agreement for the rotor loss mechanisms, slightly under-predicting the tip leakage loss but over-predicting the remainder

of the rotor losses. The main disagreement between the measurements and numerical predictions is in the primary flow, which is over-predicted in mean levels but under-predicted in size of fluctuation.

Comparison of these results with the findings from the measurements at a single vane phase of 30% shows that agreement between the measurements and the predictions is heavily dependent upon the vane phase. For example, where the stationary measurements implied that the wake entropy generation prediction was poor, the traversed measurements now show that the mean level of wake entropy generation over vane phase is reasonable. It is thus vital to measure the entire circumferential flow field to estimate the accuracy of numerical predictions.

The true averaged stage efficiency from the entropy measurements (89.9%) is now 1.2% higher than the equivalent numerically predicted value and 3.2% higher than the 86.7% efficiency value obtained, after adjustment to the same tip gap, from a cold flow rig, see Payne et al. (2003) for details. However, since we are only measuring the total entropy generated upstream of the measurement plane, the true mixed out efficiency in the present experiment will be somewhat lower than the quoted 89.9%. It is thus difficult to compare the experimental value with the model rig value, which is a fully mixed out value. The most valid comparison is with the numerical prediction. The poor agreement between experiment and prediction in terms of the level of interaction in the primary flow suggest that errors in the accuracy of the interaction prediction are the main reason for the discrepancy in the overall time-mean stage efficiency.

11. Summary and conclusions

The use of the aspirating probe to measure unsteady entropy over all vane phases has allowed the effects of blade row interaction on the loss mechanisms and the stage efficiency to be assessed. The interaction effects are strongest in the hub region, where the upstream vane wake periodically merges with the rotor lower passage vortex: termed the hub interaction phenomenon. The wake, upper passage vortex and tip leakage vortex are modulated in strength and position by vane interaction: this is a small effect in the tip region, but larger at mid-height. The degree of modulation is largely determined by the way in which the loss feature forms: hence, for example, the tip leakage vortex, which starts to form at mid-chord, is modulated less than the lower passage vortex, which starts to form at the leading edge. The magnitude of the wake entropy/R generation is in good agreement with previous measurements made with the same blade rows. The effects of vane interaction at mid-height are largely seen in a modulation in the free-stream entropy/R, with smaller variations in the height and position of the wake.

Although the predictions of the flow structure are in good agreement with the measurements, the mean stage efficiency is slightly under-predicted and the magnitude of the interaction effects is considerably under-predicted. The main cause of these differences in stage efficiency is the difference in primary flow prediction. This discrepancy between experiment and prediction is not at present understood. The differences shown in Payne et al. (2003) have been shown to be partly due to the relatively poor prediction of interaction effects. The causes of the disagreements are not yet clear.

When averaged over vane phase, the estimated stage efficiency is approximately 89.9%, with a drop of 4.2% due to the primary flow, 3.6% to the tip leakage vortex and 2.3% to the remainder of the secondary flow. The fluctuation in the stage efficiency with vane phase is large, with a standard deviation of 1.3%, showing that experimental estimates of the stage efficiency can only be made by measuring the complete flow field. Interaction effects have thus been shown to have a significant impact on the stage efficiency and must be considered carefully when attempting to improve the efficiency of blade designs. Consideration of the flow field at a single vane phase, as presented in Payne et al. (2003) is thus inadequate for accurate efficiency measurements: it is only as interaction effects are considered that the efficiency can be accurately estimated and the flow field fully understood. Future work should focus on attempting to understand why there are such large fluctuations in stage efficiency over vane phase and on improving numerical predictions of interaction effects.

Acknowledgements

The authors gratefully acknowledge the support of Kevin Grindrod as well as others from the Oxford Rotor Group. They also wish to acknowledge the support of Rolls-Royce plc, the U.K. Ministry of Defence, DTI CARAD and QinetiQ, and thank them for permission to publish this work. Stephen Payne was supported by an EPSRC studentship.

References

Ainsworth, R.W., Shultz, D.L., Davies, M.R.D., Forth, C.J.P., Hilditch, M.A., Oldfield, M.L.G., Sheard, A.G., 1988. A transient flow facility for the study of the thermofluid dynamics of a full stage turbine under engine representative conditions. ASME Paper No. 88-GT-144.

Alday, J., Osborne, D.J., Morris, B., Ng, W., Gertz, J., 1993. Flow randomness and tip losses in transonic rotors. ASME Paper No. 93-GT-189.

Binder, A., 1985. Turbulence production due to secondary vortex cutting in a turbine rotor. Journal of Engineering for Gas Turbines and Power 107, 1039–1046.

Binder, A., Schroeder, T., Hourmuziadis, J., 1989. Turbulence measurements in a multistage low-pressure turbine. Journal of Turbomachinery 111, 153–161.

Brayton, S.N., 1996. Hot wire instrumentation for unsteady aerodynamic measurements in a rotating gas turbine stage. D.Phil. Thesis, University of Oxford.

Brouckaert, J.F., 1998. Experience with a double-hot-wire aspirating probe in a transonic turbine stage. In: Proceedings from the 14th Symposium on Measuring Techniques for Transonic and Supersonic Flows in Cascades in Turbomachines, Limerick.

Bruun, H.H., 1995. Hot-wire Anemometry: Principles and Signal Analysis. Oxford University Press.

Buttsworth, D.R., Jones, T.V., Chana, K.S., 1998. Unsteady total temperature measurements downstream of a high pressure turbine. Journal of Turbomachinery 120, 760–767.

Collie, J.C., Moses, H.L., Schetz, J.A., 1992. Recent advances in simulating unsteady flow phenomena brought about by passage of shock waves in a linear turbine cascade. ASME Paper No. 92-GT-4.

Collis, D.C., Williams, M.J., 1959. Two-dimensional convection from heated wires at low Reynolds numbers. Journal of Fluid Mechanics 6, 357–389.

Denton, J.D., 1992. The calculation of three-dimensional viscous flow through multistage turbomachines. Journal of Turbomachinery 114, 18–26.

Denton, J.D., 1993. Loss mechanisms in turbomachines. Journal of Turbomachinery 115, 621–656.

Hodson, H.P., Dawes, W.N., 1998. On the interpretation of measured profile losses in unsteady wake-turbine blade interaction studies. Journal of Turbomachinery 120, 276–284.

Jennions, I.K., Adamczyk, J.J., 1997. Evaluation of the interaction losses in a transonic turbine HP rotor/LP vane configuration. Journal of Turbomachinery 119, 68–76.

Johnson, A.B., Rigby, M.J., Oldfield, M.L.G., Ainsworth, R.W., Oliver, M.J., 1989. Surface heat transfer fluctuations on a turbine rotor blade due to upstream shock wave passing. Journal of Turbomachinery 111, 105–115.

Korakianitis, T., 1993. On the propagation of viscous wakes and potential flow in axial-turbine cascades. Journal of Turbomachinery 115, 118–127.

Mee, D.J., Baines, N.C., Oldfield, M.L.G., Dickens, T.E., 1992. An examination of the contributions to loss on a transonic turbine blade in cascade. Journal of Turbomachinery 114, 155–162.

Miller, R.J., Ainsworth, R.W., 1996. An ultra-high speed traverse system for fast response aerodynamic measurements in transient flow facilities. In: Proceedings from the 13th Symposium on Measuring Techniques for Transonic and Supersonic Flows in Cascades in Turbomachines, Zurich.

Miller, R.J., Moss, R.W., Ainsworth, R.W., Harvey, N.W., 2003a. The development of turbine exit flow in a swan-necked inter-stage diffuser. ASME Paper No. 2003-GT-38174.

Miller, R.J., Moss, R.W., Ainsworth, R.W., Horwood, C.K., 2003b. Time-resolved vane–rotor interaction in a high-pressure turbine stage. Journal of Turbomachinery 125, 1–13.

Ng, W.F., Epstein, A.H., 1983. High-frequency temperature and pressure probe for unsteady compressible flows. Review of Scientific Instruments 54, 1678–1683.

Ng, W.F., Epstein, A.H., 1985. Unsteady losses in transonic compressors. Journal of Engineering for Gas Turbines and Power 107, 345–353.

Parantheon, P., Lecordier, J.C., Petit, C., 1983. Dynamic sensitivity of the constant-temperature hot-wire anemometer to temperature fluctuations. TSI Quarterly 9, 3–8.

Payne, S.J., 2001. Unsteady loss in a high pressure turbine stage. D. Phil. Thesis, University of Oxford.

Payne, S.J., Ainsworth, R.W., Miller, R.J., Moss, R.W., Harvey, N.W., 2003. Unsteady loss in a high pressure turbine stage. International Journal of Heat and Fluid Flow 24, 698–708.

Sheard, A.G., 1989. Aerodynamic and mechanical performance of a high pressure turbine stage in a transient wind tunnel. D.Phil. Thesis, University of Oxford.

Suryavamshi, N., Lakshminarayana, B., Prato, J., 1996. Aspirating probe measurements of the unsteady total temperature field downstream of an embedded stator in a multistage axial flow compressor. ASME Paper No. 96-GT-543.

Van Zante, D.E., Suder, K.L., Strazisar, A.J., Okiishi, T.H., 1995. An improved aspirating probe for total-temperature and total-pressure measurements in compressor flows. Journal of Turbomachinery 117, 642–649.

Zaccaria, M.A., Lakshminarayana, B., 1997. Unsteady flow field due to nozzle wake interaction with the rotor in an axial flow turbine: Part I—Rotor passage flow field. Journal of Turbomachinery 119, 201–213.